

Alma Mater Studiorum Università di Bologna
Archivio istituzionale della ricerca

The Role of Acidity in Terephthalic Acid Synthesis from Renewable Carbon Source

This is the final peer-reviewed author's accepted manuscript (postprint) of the following publication:

Published Version:

Trandafir M.-M., Neatu S., Bocirnea A., Counsell J., Cavani F., Florea M., et al. (2020). The Role of Acidity in Terephthalic Acid Synthesis from Renewable Carbon Source. CHEMCATCHER, 12(24), 6248-6258 [10.1002/cctc.202001388].

Availability:

This version is available at: <https://hdl.handle.net/11585/787546> since: 2023-04-23

Published:

DOI: <http://doi.org/10.1002/cctc.202001388>

Terms of use:

Some rights reserved. The terms and conditions for the reuse of this version of the manuscript are specified in the publishing policy. For all terms of use and more information see the publisher's website.

This item was downloaded from IRIS Università di Bologna (<https://cris.unibo.it/>).
When citing, please refer to the published version.

(Article begins on next page)

This is the final peer-reviewed accepted manuscript of:

Mihaela-Mirela Trandafir, Stefan Neațu, Amelia Bocîrnea, Jonathan Counsell, Fabrizio Cavani, Mihaela Florea, Florentina Neațu, "The Role of Acidity in Terephthalic Acid Synthesis from Renewable Carbon Source" ChemCatChem 2020, 12, 6248–6258

The final published version is available online at:
<https://doi.org/10.1002/cctc.202001388>

Terms of use:

Some rights reserved. The terms and conditions for the reuse of this version of the manuscript are specified in the publishing policy. For all terms of use and more information see the publisher's website.

This item was downloaded from IRIS Università di Bologna (<https://cris.unibo.it/>)

When citing, please refer to the published version.

The role of acidity in terephthalic acid synthesis from renewable carbon source

Mihaela-Mirela Trandafir,^[a] Ștefan Neațu,^[a] Amelia Bocîrnea,^[a] Jonathan Counsell,^[b] Fabrizio Cavani,^[c] Mihaela Florea,^[a] and Florentina Neațu*^[a]

[a] Dr. M.M. Trandafir, Dr. M. Florea, Dr. S. Neațu, Dr. A. Bocîrnea, Dr. F. Neațu
Institution National Institute of Materials Physics
405A Atomistilor Street, 077125 Magurele, Romania
E-mail: florentina.neatu@infim.ro

[b] Dr. J. Counsell
Kratos Analytical
Wharfside, Trafford Wharf Road, Manchester M17 1GP, UK

[c] Prof. Dr. F. Cavani
Department of Industrial Chemistry "Toso Montanari"
University of Bologna
Viale Risorgimento 4, 40136 Bologna, Italy

Supporting information for this article is given via a link at the end of the document.

Abstract: In this study, manganese-cobalt (MnCo) mixed oxide catalysts were prepared by two different routes: co-precipitation and citrate method. The structures and properties of the mixed oxide catalysts were investigated by several techniques: nitrogen adsorption-desorption isotherms, X-ray diffraction, X-ray photoelectron spectroscopy, SEM, FTIR and UV-Vis spectroscopies, temperature-programmed reduction with H₂ (H₂-TPR) and temperature-programmed desorption of NH₃ (NH₃-TPD). Their catalytic performance was investigated in the liquid-phase selective oxidation of naturally occurred *p*-cymene to terephthalic acid, as an alternative to *p*-xylene, a fossil derivative fuel component. Within this study, we demonstrate that the materials prepared by the co-precipitation method present strong acid sites that boost the oxidation rate and allow oxidation of *p*-cymene up to terephthalic acid. The co-existence of a significant number of strong acid and centers in higher oxidation state (Co³⁺) are required for these materials to be selective.

Introduction

Polyethylene terephthalate (PET) production remains one of the most important process for polyester industry with high relevance in the fibers, containers, thermoforming, manufacturing, etc.^[1] However, like PET, other TA-based polyesters and copolyesters are also widely used in the modern human life.^[2] Terephthalic acid (TA) is the key platform chemical widely used for PET synthesis, with a global annual market demand of \$45.93 billion in 2017 and a projected value of \$73.85 billion by 2026.^[3] The industrial pathway to obtain TA occurs by catalytic oxidation of *p*-xylene (PX), a fossil fuel derivative, in the toxic and harmful homogeneous Co-Mn-Br catalytic system, where the presence of bromine in a certain concentration is a prerequisite for a high TA yield.^[4]

In the context of high efficiency, the heterogenization of this catalytic system is the next step to overcome the limitation and disadvantages of using homogeneous catalysts. Nicolae *et al.*^[5] used Mn-Fe mixed oxides as heterogeneous catalysts for PX

oxidation (98% conversion) with tert-butyl hydroperoxide as the oxidant, and obtained a 93% yield in *p*-toluic acid (TOA). Further oxidation of TOA to TA is considered to be the most difficult stage for TA production.^[6] Recently, *p*-toluic acid oxidation released TA in high yield (approx. 98%) in the presence of Cu-Mn mixed oxides, using acetonitrile as the solvent and *N*-hydroxysuccinimide as a free radical promoter instead of bromine.^[7]

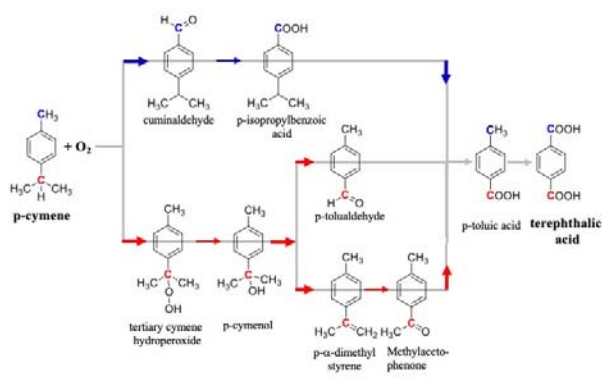
There are also studies where PX is one-step oxidized to TA, in the presence of heterogeneous catalysts, under mild reaction conditions. Deori *et al.*^[8, 9] proved the effectiveness of CeO₂ nanocrystals and nanocubes for PX oxidation to TA (61% and 99% yield, respectively), using water as the solvent. The excellent catalytic performance of CeO₂ nanocubes^[9] is attributed to the high oxygen mobility into the lattice, the contribution of the good oxygen storage capacity of ceria and the presence of numerous oxygen vacancies. Ce precursors are however expensive and the catalyst synthesis method is arduous including the use of various toxic organic compounds.

Moreover, alternative sustainable routes for TA synthesis are envisaged such as heterogeneous catalytic oxidation of *p*-cymene, an alkylbenzene synthesized by low-cost technology from biodegradable terpenes such as limonene.^[10] Recently, *p*-cymene was obtained in good yields by catalytic reforming of pyrolytic oil from scrap tyre rubber.^[11]

Even TA synthesis from *p*-cymene oxidation is not trivial.^[12] Due to the very complex reaction mechanism, it is highly desired because it represents a viable alternative to the present industrial route starting from *p*-xylene. However, there are several intermediate added value products, including TOA that can be isolated (see Scheme 1). These intermediates have various applications in the manufacture of fragrances and flavours, food sector, chemical industry and medicine,^[13] and are of significant interest.

In previous decades, several mesoporous manganese-cobalt based materials were intensively studied in catalytic oxidation reactions such as: alkane oxidation,^[14] alkyl-benzene or benzene oxidation,^[15] alcohol oxidation,^[16-18] CO oxidation^[19] and VOC

The specific surface areas (SSA) of all prepared samples determined by the Brunauer-Emmett-Teller equation using desorption data are presented in Table 1. As expected, the Mn:Co materials prepared by the citrate method have higher SSA (between 32 and 50 m² g⁻¹) than the materials prepared by the co-precipitation method (between 17 and 33 m² g⁻¹), irrespective of the Mn:Co ratio. The SEM micrographs (presented in Figure S1 in the Supporting Information) also indicate that samples prepared by the citrate method are more porous. This predictable behaviour is due to the complexation agent (citric acid) which coordinates the metal, and by its removal during calcination, increases the porosity. In this series of materials prepared by the citrate method, the decrease in Mn corresponds to an increase in surface area.



It is essential to find new compositions where the cooperative effect between the different metal ions and the lattice oxygen mobility strongly enhance activity.^[7, 25] Therefore, in this study, we propose simple and cost efficient synthesis methods for Mn/Co/O mixed oxides as co-precipitation and citrate, at different Mn:Co molar ratio. Their catalytic performance was investigated in the liquid-phase selective oxidation of naturally occurred *p*-cymene, as an alternative to *p*-xylene, a fossil derivative fuel component.

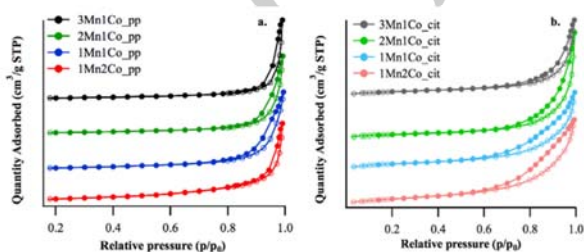
Catalysts characterisation

X-ray diffraction patterns are shown in Figure 2 for both series of Mn-Co materials. As general trends, irrespective of the preparation method used, for 1Mn2Co sample, the diffraction lines at 2θ values of 18.6° , 30.7° , 36.4° , 44.4° , 54.6° and 58.8° assigned to (111), (220), (311), (400), (422) and (511) plane reflections can be indexed to the spinel MnCo_2O_4 cubic structure (Fd3m group, PDF card No. 01-084-0482), while for 2Mn1Co sample the tetragonal form CoMn_2O_4 (spatial group I41/amd, PDF card no 00-018-408) with spinel structure^[27] was identified. In the case of the sample with equal amount of manganese and cobalt (1Mn1Co), both spinel structures MnCo_2O_4 and CoMn_2O_4 were formed; a behaviour expected considering that 1:2 ratio between the two transition metals is needed to form a spinel structure. For the sample with greater Mn amount (3Mn1Co), diffraction lines corresponding to spinel CoMn_2O_4 together with the Mn_2O_3 phase crystallized in the cubic system are identified. This behaviour can be explained due to the excess of manganese.

Under close examination however, slight differences can be observed in the diffraction patterns for the two preparation methods. Thus, the samples with Mn:Co ratio of 1:2 and 2:1 prepared by the citrate method present the corresponding spinel in the pure phase meaning MnCo_2O_4 and CoMn_2O_4 , respectively, while for the sample prepared by co-precipitation small amounts of CoMn_2O_4 or MnCo_2O_4 phase, can be identified in both cases.

It is well known that spinel cobaltite (in our case MnCo_2O_4) can be found in normal or inverse spinel structures.^[28] In our case the inverse MnCo_2O_4 structure seems to be favoured, as is detailed and confirmed further by XPS analysis. Moreover, recently it was demonstrated that for MnCo_2O_4 the inverse structure is energetically favoured.^[29]

The crystallite size determined from the XRD patterns for the prepared materials (see Table 1) are well correlated with the



2

FULL PAPER

specific surface area. In general, they are smaller (in the range of 8–13 nm) for the samples prepared by citrate (with higher SSA) and larger (in the range 11–22 nm) for the samples prepared by co-precipitation method (having lower SSA). The smaller particle

sizes obtained from the citrate method can be attributed to inhibited interparticle contact generated by the presence of the citric acid.

Table 1. Textural parameters obtained from the adsorption-desorption isotherms and crystallite size calculated from XRD for Mn-Co catalysts.

	Co-precipitation method				Citrate method			
	3Mn1Co	2Mn1Co	1Mn1Co	1Mn2Co	3Mn1Co	2Mn1Co	1Mn1Co	1Mn2Co
BET [$\text{m}^2 \text{g}^{-1}$]	33	25	17	28	32	39	42	50
Pore diameter [nm]	35	30	22	18	19	22	13	11
Average grain size ^[a] [nm]	37	48	71	44	38	31	30	24
Crystallite size ^[b] [nm]	20	16	22	11	13	10	10	8

[a] The average grain size was estimated from the surface area using the formula $d = 6000/qA$; where q is the theoretical density of the material, 4.93 mg cm^{-3} (calculated from the theoretical density of single oxides) and A is the specific surface area of the powder; [b] Determined from XRD using Debye-Scherrer equation.

UV-Vis spectra of the Mn-Co mixed oxide catalysts prepared through both co-precipitation and citrate methods are depicted in Figure 3. In the case of Mn-Co mixed oxides prepared by the co-precipitation method (see Figure 3a), all samples exhibit absorption bands in two main regions: 200–350 nm and 450–800 nm. The former region can be attributed to the allowed anionic (O^{2-})-cationic (Mn^{2+} or Mn^{3+} , Co^{3+}) charge transfer transitions produced at lower wavelengths. The latter region is related to the presence of d-d crystal field transitions on Mn^{3+} species, which are more pronounced when the Mn content increase, such in the case of Mn:Co 2:1 and 3:1 catalysts. This indicates the presence of the Mn_2O_3 phase^[30] and agrees well with XRD measurements. Similar behaviour was expected also in the case of the Mn-Co mixed oxides prepared via the citrate method (see Figure 3b).

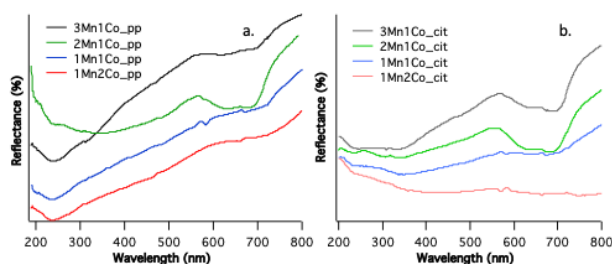


Figure 3. DR-UV-Vis spectra of the Mn-Co mixed oxides prepared by (a) co-precipitation and (b) citrate method.

However, although the samples present absorption in both regions, this time the amplitude of the absorption bands characteristic of the d-d type transitions in the case of $1\text{Mn}2\text{Co}_{\text{cit}}$ material is greatly diminished, indicating that Mn_2O_3 is either not present or is present below the detection limit of this characterization technique. These results are in good agreement with the XRD data and show that the distribution of oxides in samples is both in the form of spinel mixed oxides and single Mn_2O_3 , only when the ratio between Mn and Co species is higher than 2.

FT-IR spectra of the Mn-Co mixed oxide materials prepared by co-precipitation and citrate methods are depicted in Figure 4. In Figures 4a and 4c, in the interval $4000\text{--}2800 \text{ cm}^{-1}$, no clear differences can be observed from these spectra, only a broad absorption band located at around 3380 cm^{-1} , assigned to the presence of adsorbed water. In the interval $1800\text{--}700 \text{ cm}^{-1}$ (see Figures 4a and 4c), the Mn-Co systems display bands located at around 1635, 1520, 980 and 865 cm^{-1} assigned to angular deformation of the adsorbed water molecules, organic residues and carbonate species, respectively. What is important to note is that the band located at 865 cm^{-1} , although present in all samples, in the case of $1\text{Mn}2\text{Co}$ (both co-precipitation and citrate) it is not present. There is another broad absorption band located around 1390 cm^{-1} in the case of $3\text{Mn}1\text{Co}_{\text{pp}}$ sample, which corresponds to NO symmetric stretch mode^[31] coming from the precursor used during precipitation.

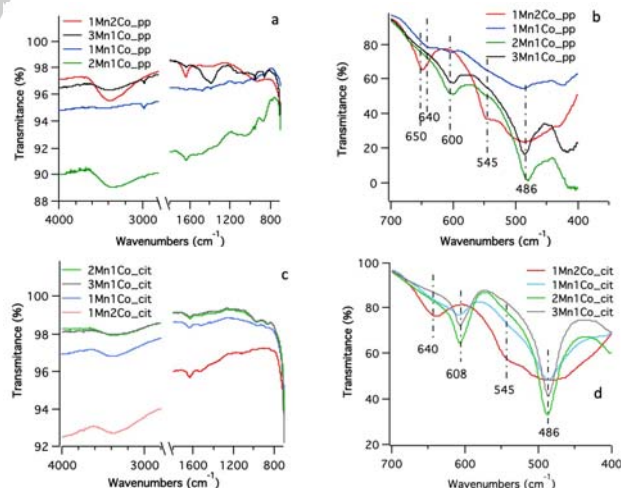


Figure 4. FT-IR spectra of Mn-Co mixed oxides prepared by co-precipitation method in the $4000\text{--}700 \text{ cm}^{-1}$ (a) and $700\text{--}500 \text{ cm}^{-1}$ region (b) and Mn-Co mixed oxides prepared by citrate method in the $4000\text{--}700 \text{ cm}^{-1}$ (c) and $700\text{--}500 \text{ cm}^{-1}$ region (d), respectively.

Figures 4b and 4d present the most important features of the Mn-Co samples, namely the metal oxide characteristic peaks of the region 700–500 cm^{-1} . It is already established that FT-IR cannot elucidate between the normal or inverse spinel structure,^[32] but can give information about the composition of the formed spinel. The bands located at around 640 cm^{-1} and 545 cm^{-1} are specific for the manganese cobaltite spinel structure and can be assigned to the vibrational stretching mode of Metal–O bonds, revealing the crystallization of MnCo_2O_4 phase.^[33] The vibrational band at 545 cm^{-1} is associated with the divalent cations found in tetrahedral environment, while the band at 640 cm^{-1} corresponds to the trivalent cations in octahedral coordination. This phase is mainly observed in the 1Mn2Co samples, but can also be observed for the sample 1Mn1Co, irrespective of the preparation method. Once with the increase of the ratio between Mn and Co, for both preparation methods, a shift of the two bands can be observed and can be associated with the spinel MnCo_2O_4 formation. The band located $\sim 600 \text{ cm}^{-1}$ can be assigned to the stretching mode of $\text{Mn}^{3+}\text{--O}$ bond found in MO_6 octahedra, while the vibrational mode at 485 cm^{-1} corresponds to the tetrahedral coordination of the divalent metals.^[34, 35] This observation is in good correlation with the XRD and UV–Vis data collected. In the samples prepared by citrate method a shift of 8 cm^{-1} of the 600 cm^{-1} band associated with $\text{Mn}^{3+}\text{--O}$ is observed, which correspond to a distortion of the octahedra due to the Jahn–Teller effect.^[35]

X-ray photoelectron spectroscopy

The surface composition of the samples was analysed by X-ray photoelectron spectroscopy. The changes that occur in the core levels of Mn and Co as a function of molar ratio between Mn and Co, depending on the preparation method, are herein discussed in detail. The experimental results were analysed in Casa XPS for the main Co $2p_{3/2}$ and Mn $2p_{3/2}$ peaks, taking into consideration the multiplet splitting and background subtraction. The highly constrained peak-fitting procedure (background subtraction, full width at half maximum, relative shifts, relative intensities and component shape), as outlined by Biesinger *et al.*, was used consistently for all spectral analysis to determine the precise oxidation states present and their relative

stoichiometries.^[36] The quantitative information was extracted after the correction with the relative sensitivity factor for the $2p_{3/2}$ peaks of the species.^[37] Figure 5 presents the normalized experimental data for each species.

The relative quantitative information extracted from the XPS analysis is summarized in Table 2.

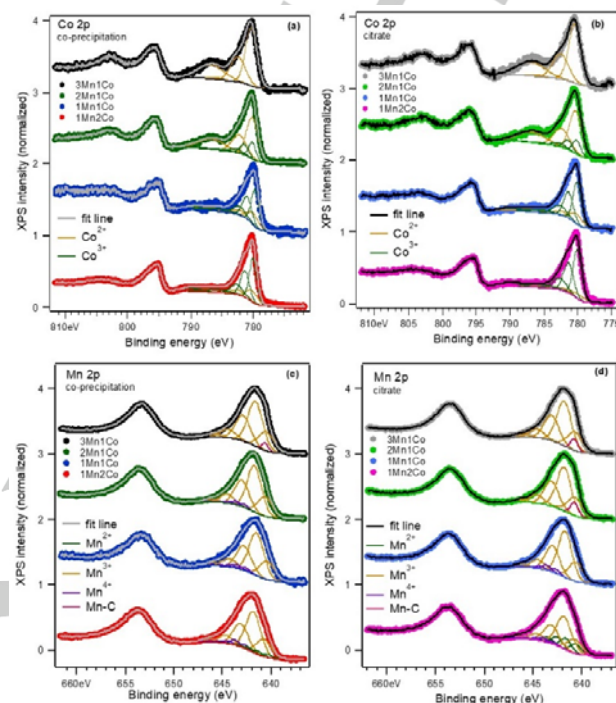


Figure 5. XPS normalized spectra of Co 2p for the catalysts prepared by (a) co-precipitation, (b) citrate method and XPS normalized spectra of Mn 2p for the catalysts prepared by (c) co-precipitation and (d) citrate method. The experimental data is represented with markers with stronger colours for the samples obtained by the precipitation method and lighter colours for the samples obtained by the citrate method. Mn^{3+} and Co^{2+} were represented with the same colour since they are part of the same spinel state.

Table 2. XPS atomic ratio found at the surface of the MnCo prepared catalysts.

Atomic ratio (XPS)	Co-precipitation method					Citrate method			
	3Mn1Co	2Mn1Co	1Mn1Co	1Mn2Co	0Mn1Co	3Mn1Co	2Mn1Co	1Mn1Co	1Mn2Co
Mn/Co	2.9	1.8	1.6	0.7	–	3.9	2.9	1.9	1.1
Mn/Co (calculated)	3.0	2.0	1.0	0.5	–	3.0	2.0	1.0	0.5
$\text{Mn}^{3+}/\text{Mn}^{2+}$	–	–	–	10.5	–	–	–	2.6	–
$\text{Mn}^{3+}/\text{Mn}^{4+}$	–	19	13.3	10.5	–	–	–	11.5	13.6
$\text{Co}^{2+}/\text{Co}^{3+}$	–	4	0.3	0.1	0.07	–	3.5	0.4	0.3
$\text{Mn}^{3+}/\text{Mn}_{\text{tot}}$	97	95	93	84	–	95	93	92	68
$\text{Co}^{3+}/\text{Co}_{\text{tot}}$	0	20	76	88	93	0	23	71	75
$\text{Co}^{3+}/\text{Mn}_{\text{tot}}$	0	0.2	0.9	1.6	–	0	0.3	1.1	2.8

O_{ad}/O^{2-}	0.38	0.37	1.05	0.47	—	0.35	0.35	1.0	0.31
$O^{2-}/(Mn+Co)$	1.31	1.32	1.12	1.2	—	6.36	6.8	4.97	7.1

The relative ratio of Mn:Co for each sample, as given by XPS, is close to the theoretical one, with the Mn content increasing accordingly.

These results show that the samples are homogeneous, with the same composition on the surface as in the bulk – i.e. no observable surface segregation was observed of either element. Moreover, the EDX analyses presented in Table S1 and Figure S2 in the Supporting Information underline the efficiency of both preparation methods, since the theoretical ratio Mn:Co is the same with experimental one.

Co 2p spectra for both preparation methods show a similar trend: with a decrease in the concentration of Co, the relative concentration of Co^{2+} increases up to the point where the Co 2p only shows the 2+ state for the 3Mn1Co samples. For the Co richer samples, the surfaces present both Co^{3+} and Co^{2+} , with different relative concentration as presented in Table 2.

The predominant state of Mn in all samples is Mn^{3+} , nevertheless for the samples containing more Co one cannot exclude the presence of Mn^{4+} in very low amounts. Also, Mn 2p spectra show the existence of the Mn^{2+} cations only for the 1Mn2Co samples in both preparation methods. The presence of Mn–C bond, was observed in 2Mn:1Co_cit (7% of the Mn 2p_{3/2} signal) and in both 3Mn1Co samples: 3% for 3Mn1Co_pp and 5% for 3Mn1Co_cit.

The presence of Mn^{2+} in the 1Mn2Co samples, obtained by both precipitation and by citrate methods, indicates the existence of the $MnCo_2O_4$ spinel, while the presence of Mn^{3+} cation shows the predominant existence of this spinel in the more efficient inverse spinel state,^[29, 38] coexisting with a small normal spinel state, as also shown by XRD. By increasing the concentration of Mn, the Mn ions start to substitute Co^{3+} positions, as revealed by the XP spectra where the relative decrease of Co^{3+} and increase of Mn^{3+} cations is observed, up to the point where all Mn 2p spectra consist of Mn^{3+} and all Co spectra consist of Co^{2+} (the reverse spinel $MnCo_2O_4$, all consist of Mn^{3+} and Co^{2+} as well as the valence of Mn_2O_3 is 3+ too). All these results are consistent with the bulk measurements of the powders by means of FT-IR and XRD.

Binding energies of O 1s are presented in Figure S3. All samples present a main peak at ~ 529.98 eV, which correspond to lattice O^{2-} of metallic oxides and a secondary peak at 531.25 eV assigned to the hydroxyl group and surface adsorbed or chemisorbed oxygen.^[18, 21] The presence of the adsorbed/chemisorbed oxygen onto the surface is usually associated with the presence of defects in the material, which are known to be beneficial for catalytic activity.^[18, 39] As observed in Table 2, for the materials prepared by co-precipitation, the ratio O_{ad}/O^{2-} is higher for the samples 1Mn1Co and 1Mn2Co indicating a higher concentration of adsorbed oxygen and probably a higher number of defects. Taking a closer look to the ratio $O^{2-}/(Mn+Co)$, which theoretically should be 1.33, for spinels we observed for the samples with higher number of defects, this ratio is lower suggesting an oxygen deficient surface, confirming the presence of increased oxygen vacancies for 1Mn1Co and 1Mn2Co.

Increased defects, meaning a higher O_{ad}/O^{2-} ratio, are observed for the sample 1Mn1Co in the series of materials prepared by the citrate method. However, for this series the ratio

$O^{2-}/(Mn+Co)$ is at least 3.5× higher than the theoretical values, most probably due to the presence of residual citrate on the surface. Residual citrate was also observed by H_2 -TPR in this series, as presented further.

H₂-TPR measurements

To investigate the redox ability of the Mn-Co mixed oxides with different molar ratios, the materials were treated with H_2 and the obtained reduction profiles are shown in Figure 6. For both catalysts series the reduction profiles indicate two reduction regions: low temperature (250–350 °C) and high temperature (400–650 °C). If we consider the pure oxides, it is known that the H_2 -TPR spectra of MnO_2 bulk nanoparticles present three reduction peaks ranging from 200 to 400 °C and are attributed to the reduction of MnO_2 to Mn_2O_3 (~ 235 °C), Mn_2O_3 to Mn_3O_4 (~ 270 °C) and Mn_3O_4 to MnO (~ 400 °C), respectively.^[40] The transformation path is as follows: $6MnO_2 + 3O \rightarrow 3Mn_2O_3 + O \rightarrow 2Mn_3O_4 + 2O \rightarrow 6MnO$ (1)

While, in the case of cobalt oxide, the reduction process occurs between 200–500 °C and can be described by the following reactions:



The first reduction step takes place at around 275 °C while the second reduction step occurs at around 350 °C.^[41]

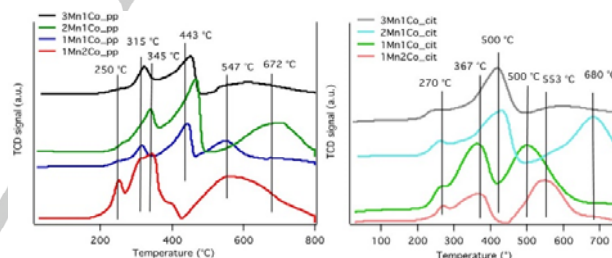


Figure 6. (a) H_2 -TPR profiles for mixed Mn-Co based materials (a) co-precipitated samples and (b) citrated samples.

For Mn-Co mixed oxides samples, the reduction profiles are different. The TPR profile for the 1Mn2Co_pp catalyst shows a low temperature peak at ~250 °C, attributed to the reduction of Mn^{4+} to Mn^{3+} , this correlates with the XPS analysis as the only catalyst with Mn^{4+} species present. The higher temperature peaks, between 315 and 450 °C, correspond to the reduction of Mn^{3+} to Mn^{2+} .^[42] The reduction temperature is shifted to higher values, as compared with the simple oxide, most probably due to a stronger interaction of Mn with the network. The broader peaks at temperatures higher than 500 °C can be attributed to the reduction of Co in a spinel-like environment to metallic Co.^[43] It is worth noting that 1Mn2Co_pp and 1Mn1Co_pp, compared with others samples, present a shift to lower temperatures indicating an enhanced reactivity of the lattice oxygen.

The reduction profiles of the samples prepared by the citrate method are quite similar to the ones prepared by co-precipitation. However, in this case, the peak at 270 °C can be attributed more

likely to the reduction of CoOOH to Co_3O_4 ,^[44] since no Mn^{4+} was observed in XPS, except for the 1Mn2Co_{cit} sample. This assumption is also supported by the $\text{O}^{2-}/(\text{Mn}+\text{Co})$ ratio calculated from XPS data, which is much higher than found for the

precipitated sample. The 1Mn1Co_{cit} and 1Mn2Co_{cit} samples present a comparable reduction profile with maxima at ~ 220, 360 °C and 500 °C, specific to the profile of the MnCo_2O_4 spinel phase.^[45] This was also observed by XRD.

Table 3. Distribution of the acidic sites for the different Mn-Co mixed oxides, as derived from TPD of NH_3 .

Catalysts	Co-precipitation method				Citrate method			
	Number of acid sites [mmol g ⁻¹]			Total number [mmol g ⁻¹]	Number of acid sites [mmol g ⁻¹]			Total number [mmol g ⁻¹]
	weak	medium	strong		weak	medium	strong	
3Mn1Co	0	0.85	0.09	0.94	0	0.47	0.08	0.55
2Mn1Co	0	0	0.43	0.43	0	0.16	0.05	0.21
1Mn1Co	0	0.05	0.46	0.51	0.01	0.15	0.01	0.17
1Mn2Co	0.09	0	0.66	0.75	0.05	0.38	0.15	0.58
0Mn1Co	0.02	0.09	0.04	0.15	–	–	–	–

No reduction peak in the high temperature region, characteristic of Co reduction, was observed for the 3Mn1Co_{cit} sample (as in the case of precipitated sample) indicating that Co is strongly bound in the spinel structure and the incorporation of manganese in greater amounts makes the corresponding samples less reducible.

In summary, the shifts to lower temperature for precipitated catalysts as compared to the citrate catalysts suggest a greater reducibility of these catalysts and a higher activity therefore expected.

NH_3 -TPD measurements

It is well known that the activities and selectivities in oxidation reactions can be relatively well explained by the acid-base properties of the catalyst. Therefore, NH_3 -TPD studies were performed to assess the density and strength of the acid sites of the Mn-Co based materials. The recorded NH_3 -TPD profiles are shown in Figure 7 and the calculated amounts of desorbed NH_3 (mmol g⁻¹) are displayed in Table 3.

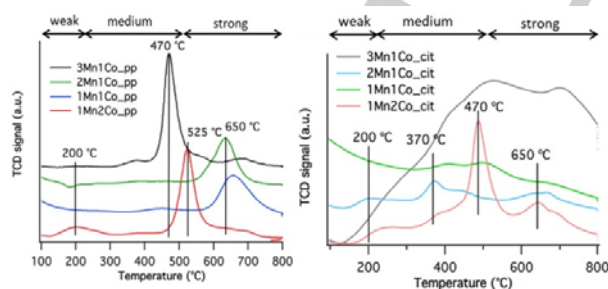


Figure 7. NH_3 -TPD profiles for mixed Mn-Co based materials (a) co-precipitated samples and (b) citrated samples.

Three distinct regions were observed which can be attributed according to the desorption temperature to three types of acidic sites: weak (100–350 °C), medium (350–500 °C) and strong (500–700 °C).^[46]

The total uptake of ammonia was higher for the catalysts prepared by precipitation, which also present a higher number of strong acid sites. Additionally, the Mn:Co molar ratio affects both the number and the strength of the acid sites (Table 3). Increasing the Mn loading (3Mn1Co) led to increased moderate strength acid sites. The total acidity increased, for both series, in the following order: 2Mn1Co < 1Mn1Co < 1Mn2Co < 3Mn1Co. In all samples prepared by co-precipitation the total acidity is at least 3 times higher than the material containing only Co (0Mn1Co, Table 3).

The acidity strength, however, shows a different trend compared with the total abundance of acid sites when changing the Mn to Co ratio, and this trend was observed for both preparation methods. A low Mn to Co ratio seems to be favourable for the formation of strong acid sites, thus for 1Mn2Co_{pp} 0.66 mmol g⁻¹ of strong acid sites are observed, while for high Mn to Co ratio (3Mn1Co) only 0.09 mmol g⁻¹. However, the single oxide containing Co possesses a very low number of strong acid sites. This underlines the importance of the co-existence of Co and Mn in a specific ratio to facilitate strong acid site appearance.

The results can also be related to Brønsted or Lewis sites. The low-temperature desorption peak below 300 °C corresponds to the NH_4^+ desorbed from Brønsted acid sites, while the Lewis acid-coordinated sites correspond to NH_3 desorbed at higher temperature.^[47] In this regard, it is obvious that all samples present higher amounts of Lewis type sites, which have a major influence in oxidation reactions. Indeed, a Lewis acid site can catalyze oxidation reactions by forming an acid-base adduct either with the substrate or with the oxidizing agent, enhancing their reactivity.^[48] All these features are well correlated to the catalytic activity results presented later.

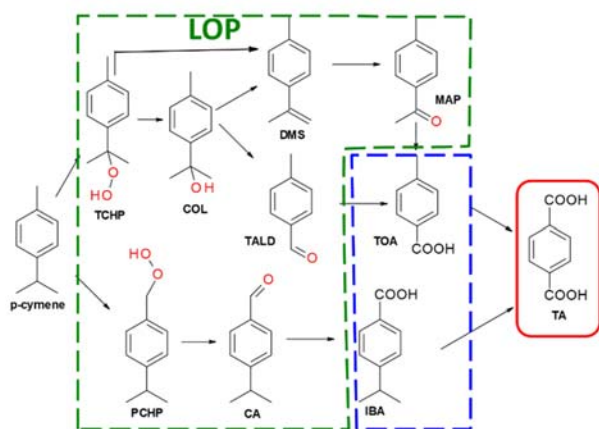
Catalytic tests

The reaction pathway for the *p*-cymene oxidation is very complex, consisting of parallel and consecutive reactions, as elsewhere described.^[49] Therefore, considering the reaction products obtained in the presence of Mn-Co mixed oxides catalysts during this study, a reaction pathway was proposed in Scheme 2.

The reaction products were classified into three main groups:

- low oxidation products (LOP) shown in Scheme 2 by the green

line and includes tertiary cymene hydroperoxide (TCHP), *p*-cymenol (COL), *p*-tolualdehyde (TALD), *p*, α -dimethylstyrene (DMS), *p*-methylacetophenone (MAP), primary cymene hydroperoxide (PCHP) and cuminaldehyde (CA), ii) advanced oxidation products (AOP) that includes *p*-toluic acid (TOA) and *p*-isopropylbenzoic acid (IBA) - shown by the blue line in Scheme 2 and iii) the most valuable product, terephthalic acid (TA), shown with the red line in Scheme 2.



Scheme 2. Main reaction products obtained by *p*-cymene oxidation.

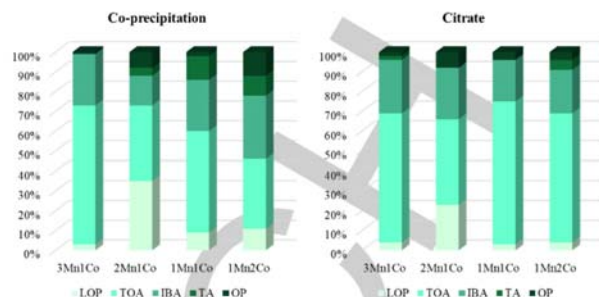


Figure 8. Catalytic performance of Mn-Co mixed oxides, in terms of product distribution, obtained during the partial oxidation of *p*-cymene, at 100% conversion of the precursor.

Table 4. Catalytic performance of MnCo-based catalysts in *p*-cymene oxidation.^[a]

Catalysts	Selectivity ^[b] [%]				
	Co-precipitation method				
	LOP	TOA	IBA	TA	Others
3Mn1Co	3	70	26	0	1
2Mn1Co	35	38	15	4	8
1Mn1Co	9	51	26	12	4
1Mn2Co	11	35	32	10	12
0Mn1Co	7	22	18	0	53
	Citrate method				
	LOP	TOA	IBA	TA	Others
	LOP	TOA	IBA	TA	Others
3Mn1Co	4	65	27	2	2
2Mn1Co	23	43	26	0	8
1Mn1Co	3	72	21	0	4
1Mn2Co	4	65	22	5	4
0Mn1Co	–	–	–	–	–

[a] Reaction conditions: 20 atm O₂, 140 °C, no solvent, O₂/*p*-cymene = 6/1, 2 mmols *p*-cymene, 16.7 mg catalyst; [b] The selectivities are presented for 100% conversion of the substrate.

There were other products (OP), in very low yields (overall < 8%, for 1Mn2Co_{pp} catalyst, where OP yield was 12%) and these are not shown in Scheme 2 for brevity.

The catalytic performances of Mn-Co mixed oxides for the liquid-phase selective oxidation of *p*-cymene, using an eco-friendly oxidation agent as molecular O₂, are summarized in Figure 8 and Table 4. All the investigated catalysts were able to completely transform *p*-cymene (100% conversion) under reaction conditions.

As a general trend, for both preparation methods employed for Mn-Co mixed oxides, it can be observed that, the AOP are formed in very high yield (65%) compared with LOP, the last ones being obtained in yields less than 35%. The *p*-cymene transformation into TA is known to occur through an autoxidation free radical mechanism.^[49] For all MnCo catalysts the major product observed was TOA, which implies the preferential oxidation of isopropyl group in detriment of the methyl group.

Such a pathway is controlled by the thermodynamic stability rule, which is specific for the classical free-radical mechanism.^[50]

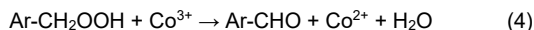
Comparing the two series of catalysts (Table 4), it can be observed that the catalysts prepared by co-precipitation result in a higher amount of AOP, and also the highest amount of TA (max 12%), than those via citrate (max 5% TA). Several studies, such as cyclohexanone oxidation to adipic acid^[51] and autoxidation of *p*-xylene to benzaldehyde^[52] over Mn/Co catalysts emphasized the role of acidity in the autoxidation mechanism and TA formation. Thus, stronger acidity leads to better activity.

Therefore, by analysing the acid centers found in the most efficient materials, a larger number of strong acid centers in the materials prepared by the co-precipitation method (0.46 and 0.66 mmol g⁻¹ for 1Mn1Co_{pp} and 1Mn2Co_{pp}, respectively) were evidenced compared to those prepared by the citrate method (0.15 mmol g⁻¹ for 1Mn2Co_{cit}) (see Table 3). These strong acid centers increase the oxidation rate by activating the C–H bonds in aromatic hydrocarbons much more easily, which may explain

FULL PAPER

the different behaviour of the catalysts prepared by the two methods. Moreover, the precipitated catalysts present a shift to lower temperature in H₂-TPR analyses as compared to citrate ones suggesting better reducibility of these catalysts, and as such, higher activity was observed indicating a higher ability to change the oxidation state of metallic components.

In the series of materials prepared by the co-precipitation method the best selectivity in TA was obtained for 1Mn1Co_{pp} (12%) and 1Mn2Co_{pp} (10%), while for the materials prepared by citrate the most selective catalyst was 1Mn2Co_{cit} (5%, Table 4). Beside the fact that the best catalysts have the highest number of strong acid sites (see Table 3), they also have in the structure as main phase MnCo₂O₄, which corresponds to a significant amount of Co³⁺. This seems to play an important role and improves selectivity to advanced oxidation products such as TA. Thus, Co³⁺ could have a role in the initiation of a chain reaction and also, as revealed by W. Partenheimer could play a role in the dehydration reaction of peroxide to form the aldehyde (eq. 4), as Lewis acid.^[52]



This agrees well with NH₃-TPD analysis, if we consider the acid sites distribution as Brønsted and Lewis as a function of the desorption temperature.

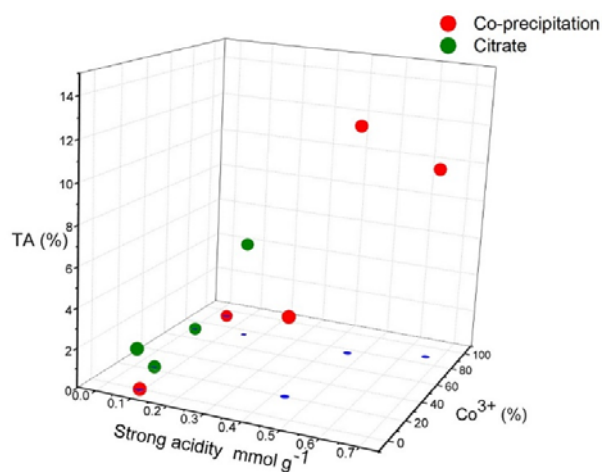


Figure 9. Dependence of TA selectivity on strong acidity and Co³⁺ content. The blue dots represent the xy projection of TA selectivity (strong acidity function of Co³⁺ content).

Taking into account that the best catalysts are those containing in their structure a high amount of Co³⁺, we have prepared by co-precipitation a sample containing only Co using the same procedure as for the other samples. As observed in Figure S5 in the Supporting Information the sample presents a spinel structure CoCo₂O₄ (PDF card 00-042-1467) and a high content of Co³⁺ ions (93%) of the total amount of Co species identified according to the XPS data (Figure S6 in the Supporting Information and Table 2). The material was tested for the oxidation of *p*-cymene and the results show a low selectivity towards AOP (40%), demonstrating that the presence of Co³⁺ is not sufficient to perform the oxidation toward TOA, TA or/and IBA in significant abundance. The acidity of Co₃O₄ is low (0.15 mmol

g⁻¹, Table 3) and the presence of strong acid is insignificant (Figure S8 in the Supporting Information), indicating that the number and strength of acidity is a key feature for the catalysts to perform the oxidation of *p*-cymene to TA.

Figure 9 depicts the dependence of TA selectivity on strong acidity and Co³⁺ content, irrespective of the preparation method employed. It is obvious that the presence of just strong acid sites is not enough to obtain a very good selectivity (see Figure 9), as is the case for 2Mn1Co_{pp}, for which LOP were obtained in the highest amounts (35%). In this case the predominant structural phase is CoMn₂O₄, which was shown to have a high abundance of strong acid sites, but low Co³⁺ (20%, Table 2). Conversely, for 1Mn1Co_{cit} material, where a low abundance of strong acids sites and a high amount of Co³⁺ is present, high amounts of TOA (72%) along with IBA (21%) was formed, but not TA, indicating the importance of the preparation method.

Catalysts with a favourable balance between the high abundance of strong acid sites and the high concentration of Co³⁺ as 1Mn1Co_{pp} and 1Mn2Co_{pp}, according to NH₃-TPD and XPS (see Tables 2 and 3) are able to convert *p*-cymene in AOP (selectivity > 67%) and TA (selectivity > 10%). These observations validate the hypothesis that the co-existence of a significant number of strong acid and centers in higher oxidation state (Co³⁺) are required for these materials to be selective. Moreover, the strength of the acid sites is also important and we observe that their presence is a prerequisite to obtain TA. Low amounts of TA (max. 5%) were obtained for the materials prepared by the citrate method, which possess fewer strong acid sites (0.01-0.15 mmol g⁻¹, Figure 9). Our results are in agreement also with other studies^[48] which claim that the catalytic performance in the oxidation reaction of hydrocarbons strongly depends on the type of catalytic site, which may be an assembly of an acid/base site and the redox properties of the metallic atom.

The total acidity of the prepared materials increases with the increase of Mn, as can be seen in Table 3, where by replacing Co with Mn the total acidity modifies from 0.15 to 0.95 mmol g⁻¹ for 0Mn1Co_{pp} and 3Mn1Co_{pp}, respectively. However, the increase of the Mn content is in detriment to the high number of strong acids sites, which decrease from 0.66 to 0.09 mmol g⁻¹ for 1Mn2Co_{pp} and 3Mn1Co_{pp}, respectively. It is very possible that the co-existence of Co³⁺ and Mn in a specific ratio play a role in facilitating strong acid site appearance, since the atomic ratio of Co³⁺/Mn, as determined by XPS, has the same linear dependency as the number of strong acid sites determined by NH₃-TPD (see Figure 10). Thus, a high Co³⁺/Mn ratio is well correlated with the presence of high amount of strong acid sites. Such cooperative effect of Co and Mn was also observed in other studies, e.g. the TPR analysis evidenced an increased oxide-reduction sites that with high advantage for catalytic VOCs oxidation^[20, 53] or from TPO was evidenced a higher oxygen absorption capacity of materials when Co and Mn were together in the vanillin synthesis through oxidation.^[17]

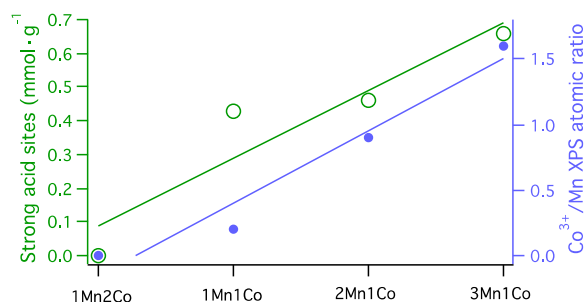


Figure 10. Linear dependence of strong acid sites vs. Co^{3+}/Mn XPS atomic ratio of MnCo materials prepared by co-precipitation.

Comparing the most efficient two samples 1Mn2Co_{pp} and 1Mn1Co_{pp} only from the perspective of strong acidity and Co^{3+} amount we expected that 1Mn2Co_{pp} presents the highest selectivity in TA, which is not the case. However, taking in account that the XPS analysis revealed for 1Mn1Co_{pp} the presence of both defects and oxygen vacancies (different $\text{O}_{ad}/\text{O}^{2-}$ ratio) in larger amount than for the 1Mn2Co_{pp} sample, the higher selectivity to TA is justified since they play a key role in the initiation chain reaction.

One final comment, we should also stress out that the preparation method is very important. As observed for the citrate method, a lower number of total/strong acid sites are obtained in comparison with the co-precipitation method, probably due to a different dispersion of Mn and Co in the material. Indeed, this is also confirmed by other studies which have used hydrothermal methods to prepare the 1Mn2Co material and obtained a mixture of Co_3O_4 , Mn_3O_4 and an unexpected CoMn_2O_4 spinel phase.^[17] It is known that the use of citric acid prevent agglomeration,^[54] and generates a homogeneous dispersion, while by co-precipitation a heterogeneous dispersion of the Mn and Co in the material can be found. In our case, the preparation method induces different acidity and spinel phases, co-precipitation leading to a heterogeneous dispersion, that induce a higher number of acids sites, which are extremely important for the catalytic activity.

Stability tests

Stability tests were performed over one of the best catalysts, 1Mn2Co_{pp}. Three consecutive runs were performed (see Table S2). The catalyst was recovered by centrifugation using a mixture of water and ethanol with a volumetric ratio of 1:1. Before reuse, the catalyst was dried 2h at mild temperature (60 °C). As can be observed in Table S2, the conversion slightly decreases upon the three cycles, with a total loss of 9%, while the selectivity to TOA, IBA and TA remains almost constant, demonstrating the stability of this catalyst.

Conclusion

TA can be obtained by oxidation of *p*-cymene using MnCo oxides as catalysts and no others additives. This study shows that the preparation method is essential in obtaining active heterogeneous materials that encounter the properties found in the classical homogeneous Co/Mn system, which are able to initiate the

autoxidation of *p*-cymene up to TA. We established that an efficient material should present metal in higher oxidation states like Co^{3+} , in strong liaison with strong acids and defects/oxygen vacancies. Moreover, in this particular case when a certain amount of Mn is present in the material, generation of strong acid centers occurs preferentially. From the two preparation methods used, co-precipitation and citrate method, the former method succeed to lead to materials with proper characteristics for the autoxidation of *p*-cymene to TA. Optimization of the catalytic features highlighted in this paper, can foster the selectivity to TA but make the subject of another study.

Experimental Section

Catalyst preparation

The Mn and Co mixed oxides were synthesized by two techniques: co-precipitation and citrate method. The following materials were purchased from Merck (the former Sigma Aldrich) and used as received: manganese (II) nitrate tetrahydrate ($\geq 98\%$), cobalt (II) nitrate hexahydrate ($\geq 98\%$), citric acid anhydrous, and sodium hydroxide pellets. Only MilliQ ultrapure water with a resistivity of 18.2 MΩ cm, measured at 25 °C, was used. To prepare the Mn and Co mixed oxides through co-precipitation method, the aqueous solutions of the Mn and Co precursors were mixed under magnetic stirring. The mixture was precipitated with NaOH solution (0.2 M), heated at 90 °C and stirred continuously for one hour. The precipitate was separated from the mixture by filtration using a Buchner funnel and a vacuum pump. The solid was dried at 100 °C for 24 h and calcined at 460 °C for 5 h, with a heating rate of 5 °C min⁻¹. Thus, Mn/Co in the molar ratios of 1:1, 1:2, 2:1 and 3:1 were prepared. Mn/Co mixed oxides with molar ratios varying from 1:1, 1:2, 2:1, 3:1, were also prepared by the citrate method. Stoichiometric amounts of manganese (II) nitrate and cobalt (II) nitrate were dissolved in MilliQ water at 60 °C to form a clear solution and then mixed together, under vigorous stirring. Citric acid was added to this mixture with 20 vol.% excess. The solution was stirred for 1h at 60 °C and then the solvent was removed using a rotary evaporator, at 60 °C, until a gel was formed. The slurry formed was dried under vacuum at 60 °C for 5h and overnight at 120 °C, in the absence of vacuum. The obtained powder was ground in a mortar and calcined at 450 °C for 5 h. For sake of comparison, single Co_3O_4 was prepared by precipitation using the precipitation procedure. The samples were denoted as following: XMnYCo_{pp} or XMnYCo_{cit} , where X and Y represent the mole number of Mn and Co, respectively; *pp* is used for the materials prepared by the co-precipitation method, while *cit* was used for the citrate method.

Catalyst characterization

The solids were investigated by means of optical, vibrational, structural, textural, morphological and surface properties characterization using different techniques, like: UV-Vis spectroscopy (in DRS mode), FTIR spectroscopy (in DRIFT mode), powder X-ray diffraction (XRD), N_2 adsorption-desorption isotherms (BET formalism), scanning electron microscopy (SEM) and X-ray photoelectron spectroscopy (XPS), temperature-programmed reduction with H_2 (H_2 -TPR) and temperature-programmed desorption of NH_3 (NH_3 -TPD), respectively. Diffuse reflectance spectra (DRS) in the range 200-800 nm were collected under ambient conditions on a UV3600 UV-Vis spectrometer from Shimadzu equipped with Shimadzu ISR-3100 integrating sphere attachment, with barium sulfate (Merck) as baseline. Vibrational properties of our samples were investigated on a PerkinElmer Spectrum Two FT-IR spectrometer equipped with a universal attenuated total reflection (UATR) accessory containing a diamond/ZnSe crystal (1 reflection). FT-IR spectra were recorded at a 4 cm⁻¹ spectral resolution in the middle infrared (MIR) range of 4000-500 cm⁻¹. XRD characterization was performed on a Bruker-AXS D8 Advance diffractometer equipped with a LynxEye one-dimensional

detector and using the Cu K α radiation (0.1541 nm). A scanning speed of 0.10 degrees per minute in the 2 θ range of 15–70 degrees was employed in all cases. Using the XRD diffraction data, the crystallite sizes of cobalt oxides were able to be estimated using the Scherrer equation. The investigation of the textural properties of our samples was analysed with the adsorption-desorption isotherms of N $_2$ on a Micromeritics instrument (ASAP 2010). The procedure implies the adsorption of N $_2$ at the nominal temperature of liquid nitrogen (\sim 196 °C) at a wide relative pressure range from 0.01 to 0.995 on previously out-gassed samples (at 150 °C under helium atmosphere for 5 h). The specific surface areas and the pore size distributions of our samples were calculated using the Brunauer-Emmett-Teller (BET) formalism^[55] and Barrett-Joyner-Halenda (BJH) method,^[56] respectively. SEM images of our samples were obtained using a Vega II LMU electron microscope model from Tescan equipped with a spectrometer of energy dispersion of X-ray (EDX) Bruker Quantax 200. The operational parameters were: accelerating voltage 30 kV, measuring time 1200 s, working distance \sim 17 mm, counting rate 0.4 kcps. All the XPS measurements were performed on Kratos Ultra DLD Setup using Al K α radiation (1486.74 eV) produced by a monochromatized X-ray source operating on a total power of 300 W (12.0 kV x 25 mA), on a routine base pressure of 1×10^{-9} Pa. Photoelectrons were collected using the Kratos hemispherical energy analyser operated in fixed analyser transmission mode with pass energy of 20 eV. Additionally, an electron flood gun operating at 1 eV electron energy and 0.1 mA current was used to avoid sample charging during measurements. The above parameters were optimized in order to obtain the C 1s peak of the adventitious carbon contamination of the sample at 284.60 ± 0.05 eV. H $_2$ -TPR was conducted on a chemisorption analyser (Porotec instrument) equipped with a thermal conductivity detector (TCD). The samples (50–60 mg) were firstly outgassed at 200 °C for 1 h in He flow (20 mL min $^{-1}$) and after that cooled to room temperature. Then the samples were heated up to 700 °C under a 5% H $_2$ /Ar gas flow (20 mL min $^{-1}$) at a rate of 5 °C min $^{-1}$. NH $_3$ -TPD was performed to determine the acidity of the catalysts using a Porotec apparatus equipped with a programmable temperature furnace and TCD detector. All catalysts (0.05 g) were treated for 1 h with 20 mL min $^{-1}$ He at 250 °C for cleaning the surface. After that, 10% NH $_3$ /He (20 mL min $^{-1}$) has been passed for 10 min at 100 °C and purged with 20 mL min $^{-1}$ He for 2 h. Under the same flow of He, the temperature was raised from 100 °C to 700 °C with 10 °C min $^{-1}$, and the desorbed ammonia was analysed.

Catalytic test

All oxidations were performed with molecular oxygen, thus *p*-cymene (2 mmol) and the catalyst (16.7 mg) were loaded in a 25 mL stainless steel autoclave, under O $_2$ pressure (20 bar). The experiments were performed at 140 °C for 6 h. The reaction products were collected with concentrated NaOH solution (1M) to afford complete dissolution of aromatic mono-/di-carboxylic acids. The products were precipitated with concentrated H $_2$ SO $_4$ (98%). The precipitate was thoroughly washed with water and the filtrate was washed three times with CH $_2$ Cl $_2$ to collect all the products. The precipitate and the organic phase were mixed together and the products concentrated under vacuum at 60 °C. The products were analysed by 1 H- and 13 C-NMR using a Bruker Fourier 300 MHz spectrometer.

Acknowledgements

This work was supported by a grant of the Romanian National Authority for Scientific Research and Innovation, CNCS/CCCI-UEFISCDI, project number PN-III-P2-2.1-PED-2016-1429. Financial support from Romanian Ministry of Research and Innovation through the Core Program PN18-11 and The University of Bucharest - UniRem project no. 244 are gratefully acknowledged.

Keywords: Mn-Co mixed oxides • terephthalic acid synthesis • *p*-cymene oxidation • autooxidation • strong acidity

- [1] a) V. A. Adamian, W. H. Gong in *Liquid Phase Aerobic Oxidation Catalysts: Industrial Applications and Academic Perspectives* (Eds.: S. S. Stahl, P. L. Alsters), Wiley-VCH Verlag GmbH & Co. KGaA, Weinheim, Germany **2016**, pp. 41–66; b) R. A. F. Tomás, J. C. M. Bordado, J. F. P. Gomes, *Chem. Rev.* **2013**, *113*, 7421–7469.
- [2] a) X. -G. Li, M. -R. Huang, G. -H. Guan, T. Sun, *Polym. Int.* **1998**, *46*, 289–297; b) X. -G. Li, G. Song, M. -R. Huang, *ACS Sustainable Chem. Eng.* **2017**, *5*, 2181–2195; c) X. -G. Li, G. Song, M. -R. Huang, Y. -B. Xie, *ACS Sustainable Chem. Eng.* **2018**, *6*, 9074–9085; d) X. -G. Li, G. Song, M. -R. Huang, T. Ohara, H. Yamada, T. Umeyama, T. Higashino, H. Imahori, *J. Clean. Prod.* **2019**, *206*, 483–497.
- [3] www.globalnewswire.com
- [4] a) K. A. Goulas, M. Shiramizu, J. R. Lattner, B. Saha, D. G. Vlachos, *Appl. Catal. A* **2018**, *552*, 98–104; b) M. Ghiaci, M. Mostajeran, A. Gil, *Ind. Eng. Chem. Res.* **2012**, *51*, 15821–15831.
- [5] S. Nicolae, F. Neatu, M. Florea, *C. R. Chim.* **2018**, *21*, 354–361.
- [6] a) J. W. Kwak, J. S. Lee, K. H. Lee, *Appl. Catal. A* **2009**, *358*, 54–58; b) Y. Tashiro, T. Iwahama, S. Sakaguchi, Y. Ishii, *Adv. Synth. Catal.* **2001**, *343*, 220–225.
- [7] M. A. Betiha, N. G. Kandile, A. M. Badawi, S. M. Solymann, A. S. Afify, *New J. Chem.* **2018**, *42*, 6343–6353.
- [8] K. Deori, D. Gupta, B. Saha, S. K. Awasthi, S. Deka, *J. Mater. Chem. A* **2013**, *1*, 7091–7099.
- [9] K. Deori, D. Gupta, B. Saha, S. Deka, *ACS Catal.* **2014**, *4*, 3169–3179.
- [10] a) M. Kamitsos, G. D. Panagiotou, K. S. Triantafyllidis, K. Bourikas, A. Lycourghiotis, C. Kordulis, *Appl. Catal. A* **2014**, *474*, 224–229; b) M. A. Martin-Luengo, M. Yates, M. J. Martínez Domingo, B. Casal, M. Iglesias, M. Esteban, E. Ruiz-Hitzky, *Appl. Catal. B* **2008**, *81*, 218–224; c) J. L. F. Monteiro, C. O. Veloso, *Top. Catal.* **2004**, *27*, 169–180.
- [11] C. Tavera-Ruiz, P. Gauthier-Maradei, M. Capron, D. Ferreira-Beltran, C. Palencia-Blanco, J. C. Morin, F. Dumeignil, *Waste Biomass Valorization* **2019**, *10*, 3057–3069.
- [12] J. C. Van der Waal, E. Mazoyer, H. J. Baars, G. -J. M. Gruter in *Liquid Phase Aerobic Oxidation Catalysts: Industrial Applications and Academic Perspectives* (Eds.: S. S. Stahl, P. L. Alsters), Wiley-VCH Verlag GmbH & Co. KGaA, Weinheim, Germany **2016**, pp. 311–329.
- [13] a) K. Nair, D. P. Sawant, G. V. Shanbhag, S. B. Halligudi, *Catal. Commun.* **2004**, *5*, 9–13; b) M. Colonna, C. Berti, M. Fiorini, E. Binassi, M. Mazzacurati, M. Vannini, S. Karanam, *Green Chem.* **2011**, *13*, 2543–2548.
- [14] a) X. Li, T. Lunkenbein, V. Pfeifer, M. Jastak, P. K. Nielsen, F. Girgsdies, A. Knop-Gericke, F. Rosowski, R. Schlögl, A. Trunschke, *Angew. Chem. Int. Ed.* **2016**, *55*, 4092–4096; b) S.-Y. Chen, W. Tang, J. He, R. Miao, H.-J. Lin, W. Song, S. Wang, P.-X. Gao, Steven L. Suib, *J. Mater. Chem. A* **2018**, *6*, 19047–19057.
- [15] a) N. Masunga, B. P. Doyle, E. Carleschi, R. Meijboom, *Appl. Catal. A: Gen.* **2018**, *559*, 175–186; b) X. Wang, Y. Liu, T. Zhang, Y. Luo, Z. Lan, K. Zhang, J. Zuo, L. Jiang, R. Wang, *ACS Catal.* **2017**, *7*, 1626–1636; c) W. h. Yu, C. h. Zhou, D. s. Tong, T. n. Xu, *J. Mol. Catal. A Chem.* **2012**, *365*, 194–202.
- [16] a) S. Biswas, B. Dutta, A. Mannodi-Kanakkithodi, R. Clarke, W. Song, R. Ramprasad, S. L. Suib, *Chem. Commun.* **2017**, *53*, 11751–11754; b) W. Gac, M. Greluk, G. Slowik, S. Turczyniak-Surdacka, *Appl. Surf. Sci.* **2018**, *440*, 1047–1062.
- [17] A. Jha, K. R. Patil, C. V. Rode, *ChemPlusChem* **2013**, *78*, 1384–1392.
- [18] Y. Huang, K. Ye, H. Li, W. Fan, F. Zhao, Y. Zhang, H. Ji, *Nano Res.* **2016**, *9*, 3881–3892.
- [19] C. Liu, L. Gong, R. Dai, M. Lu, T. Sun, Q. Liu, X. Huang, Z. Huang, *Solid State Sci.* **2017**, *71*, 69–74.
- [20] M. H. Castaño, R. Molina, S. Moreno, *Appl. Catal. A* **2015**, *492*, 48–59.
- [21] Z.-Y. Tian, P. H. Tchoua Ngamou, V. Vannier, K. Kohse-Höinghaus, N. Bahlawane, *Appl. Catal. B* **2012**, *117–118*, 125–134.
- [22] Y. Du, Q. Meng, J. Wang, J. Yan, H. Fan, Y. Liu, H. Dai, *Microporous Mesoporous Mater.* **2012**, *162*, 199–206.
- [23] a) B. Dutta, V. Sharma, N. Sassu, Y. Dang, C. Weerakkody, J. Macharia, R. Miao, A. R. Howell, S. L. Suib, *Green Chem.* **2017**, *19*, 5350–5355; b) S. L. Suib, *J. Mater. Chem.* **2008**, *18*, 1623–1631.
- [24] a) P. van Helden, J.-A. van den Berg, C. J. Weststrate, *ACS Catal.* **2012**, *2*, 1097–1107; b) N. Bingwa, S. Bewana, M. J. Ndolomingo, N. Mawila, B. Mogudi, P. Ncube, E. Carleschi, B. P. Doyle, M. Haumann, R. Meijboom, *Appl. Catal. A* **2018**, *555*, 189–195.
- [25] B. Dutta, S. March, L. Achola, S. Sahoo, J. He, A. Shirazi Amin, Y. Wu, S. Poges, S. Pamir Alpaya, S. L. Suib, *Green Chem.* **2018**, *20*, 3180–3185.
- [26] S. Lowell, J. E. Shields, M. A. Thomas, M. Thommes, *Characterization of porous solids and powders: Surface area, pore size and density* Springer, Dordrecht, Boston, London **2004**.
- [27] J. Li, S. Xiong, X. Li, Y. Qian, *Nanoscale* **2013**, *5*, 2054–2054; Y. Xu, X. Wang, C. An, Y. Wang, L. Jiao, H. Yuan, *J. Mater. Chem. A* **2014**, *2*, 16480–16488.
- [28] G. Wu, J. Wang, W. Ding, Y. Nie, L. Li, X. Qi, S. Chen, Z. Wei, *Angew. Chem. Int. Ed.* **2016**, *55*, 1340–1344.

- [29] S. Liu, D. Ni, H.-F. Li, K. N. Hui, C.-Y. Ouyang, S. C. Jun, *J. Mater. Chem. A* **2018**, *6*, 10674-10685.
- [30] H. Chen, J. He, *J. Phys. Chem. C* **2008**, *112*, 17540-17545.
- [31] Z. A. Ansari, S. Khalid, A. A. Khan, H. Fouad, S. G. Ansari, *Sens. Lett.* **2014**, *12*, 1495-1501.
- [32] W. B. White, B. A. DeAngelis, *Spectrochim. Acta A Mol. Spectrosc.* **1967**, *23*, 985-995.
- [33] a) M. Velmurugan, S.-M. Chen, *Sci. Rep.* **2017**, *7*, 653; b) R. M. Rojas, E. Vila, O. García, J. L. M. de Vidales, *J. Mater. Chem.* **1994**, *4*, 1635-1639.
- [34] a) M. Bijelić, X. Liu, Q. Sun, A. B. Djurišić, M. H. Xie, A. M. C. Ng, C. Suchomski, I. Djerdj, Ž. Skoko, J. Popović, *J. Mater. Chem. A* **2015**, *3*, 14759-14767; b) L. Malavasi, P. Galinetto, M. C. Mozzati, C. B. Azzoni, G. Flor, *Phys. Chem. Chem. Phys.* **2002**, *4*, 3876-3880; c) S. A. Hosseini, D. Salari, A. Niaei, F. Deganello, G. Pantaleo, P. Hojati, *J. Environ. Sci. Health A* **2011**, *46*, 291-297.
- [35] X. Wang, Q. Cui, Y. Pan, G. Zou, *J. Alloys Compd.* **2003**, *354*, 91-94.
- [36] M. C. Biesinger, B. P. Payne, A. P. Grosvenor, L. W. M. Lau, A. R. Gerson, R. S. C. Smart, *Appl. Surf. Sci.* **2011**, *257*, 2717-2730.
- [37] <http://www.xpsfitting.com/>
- [38] K. J. Kim, J. W. Heo, *J. Korean Phys. Soc.* **2012**, *60*, 1376-1380.
- [39] Z. Li, M. Meng, Y. Zha, F. Dai, T. Hu, Y. Xie, J. Zhang, *Appl. Catal. B* **2012**, *121-122*, 65-74.
- [40] X. Tang, J. Li, L. Sun, J. Hao, *Appl. Catal. B* **2010**, *99*, 156-162.
- [41] C. W. Tang, C. B. Wang, S. H. Chien, *Thermochim. Acta* **2008**, *473*, 68-73.
- [42] F. Liu, H. He, Y. Ding, C. Zhang, *Appl. Catal. B* **2009**, *93*, 194-204.
- [43] J.-F. Lamontier, A.-B. Boutoundou, C. Gennequin, M. J. Pérez-Zurita, S. Siffert, A. Aboukais, *Catal. Lett.* **2007**, *118*, 165-172.
- [44] J. van de Loosdrecht, S. Barradas, E. A. Caricato, N. G. Ngwenya, P. S. Nkwanyana, M. A. S. Rawat, B. H. Sigwebela, P. J. van Berge, J. L. Visagie, *Top. Catal.* **2003**, *26*, 121-127.
- [45] X. Huang, H. Zheng, G. Lu, P. Wang, L. Xing, J. Wang, G. Wang, *ACS Sustain. Chem. Eng.* **2019**, *7*, 1169-1177.
- [46] V. Middelkoop, T. Slater, M. Florea, F. Neațu, S. Danaci, V. Onyenkeadi, K. Boonen, B. Saha, I.-A. Baragau, S. Kellici, *J. Clean. Prod.* **2019**, *214*, 606-614.
- [47] D. Wang, Y. Jangjou, Y. Liu, M. K. Sharma, J. Luo, J. Li, K. Kamasamudram, W. S. Epling, *Appl. Catal. B* **2015**, *165*, 438-445; S. M. Lee, K. H. Park, S. S. Kim, D. W. Kwon, S. C. Hong, *J. Air Waste Manag. Assoc.* **2012**, *62*, 1085-1092.
- [48] A. Corma, H. García, *Chem. Rev.* **2002**, *102*, 3837-3892.
- [49] F. Neațu, G. Culică, M. Florea, V. I. Parvulescu, F. Cavani, *ChemSusChem* **2016**, *9*, 3102-3112.
- [50] A. Onopchenko, J. G. D. Schulz, R. Seekircher, *J. Org. Chem.* **1972**, *37*, 1414-1417.
- [51] a) F. Cavani, L. Ferroni, A. Frattini, C. Lucarelli, A. Mazzini, K. Raabova, S. Alini, P. Accorinti, P. Babini, *Appl. Catal. A* **2011**, *391*, 118-124; b) A. Shimizu, K. Tanaka, H. Ogawa, Y. Matsuoka, M. Fujimori, Y. Nagamori, H. Hamachi, K. Kimura, *Bull. Chem. Soc. Jpn.* **2003**, *76*, 1993-2001.
- [52] a) W. Partenheimer, *J. Mol. Catal. A Chem.* **2003**, *206*, 105-119; b) W. Partenheimer, *J. Mol. Catal. A Chem.* **2003**, *206*, 131-144.
- [53] D. A. Aguilera, A. Perez, R. Molina, S. Moreno, *Appl. Catal. B* **2011**, *104*, 144-150.
- [54] a) M. A. Dheyab, A. A. Aziz, M. S. Jameel, O. A. Noqta, P. M. Khaniabadi, B. Mehrdel, *Sci. Rep.* **2020**, *10*, 10793; b) Q. Xu, D. -P. Huang, W. Chen, J. -H. Lee, H. Wang, R. -Z. Yuan, *Scr. Mater.* **2004**, *50*, 165-170.
- [55] S. Brunauer, P. H. Emmett, E. Teller, *J. Am. Chem. Soc.* **1938**, *60*, 309-319.
- [56] E. P. Barrett, L. G. Joyner, P. P. Halenda, *J. Am. Chem. Soc.* **1951**, *73*, 373-380.

Entry for the Table of Contents

Insert graphic for Table of Contents here.



Strong acid sites promote terephthalic acid synthesis. Tuning the preparation method can generate different acidity in heterogenous catalysts. MnCo mixed oxides synthesized by co-precipitation are able to autoxidize p-cymene without any additives.